

In Situ Control of CVD Synthesis of Graphene Film on Nickel Foil

Maxim G. Rybin,* Ivan I. Kondrashov, Anatoliy S. Pozharov, Van Chuc Nguyen, Ngoc Minh Phan, and Elena D. Obraztsova

Here we present a detailed study of the chemical vapor deposition (CVD) method used in a real-time regime for graphene film fabrication on nickel foils. Thin films with a wide range of thicknesses (from 3 up to 53 layers and more) have been obtained. A home-made cold-wall chamber for CVD realization is demonstrated in this work. It is supplied with tools for in situ monitoring the temperature-dependent electrical resistance of nickel substrate to obtain a desired number of graphene layers in the sample synthesized. An area of $1 \times 1 \text{ cm}^2$ appeared to be covered by graphene. Raman spectroscopy and optical absorption spectroscopy are used to estimate the quality of graphene films fabricated and the graphene layer number.

1. Introduction

Graphene films have a great potential in electronics, photonics and optics.^[1–10] During last years, the chemical vapor deposition (CVD) method for graphene synthesis had a breakthrough as an approach to produce high-quality and large-scale samples of two-dimensional carbon material. A variety of different catalytic metal substrates can be used for the decomposition of carbonaceous gas and the formation of graphene film. A review of graphene CVD synthesis on metal substrates is presented in Refs. [11–13]. The nickel substrate is one of the most popular catalytic substrates for graphene synthesis because

the mechanism of graphite formation on nickel already has been investigated long time ago.^[14–16] Nowadays, the production of graphene film with a desired thickness is an actual problem. There is a lot of publications concerning the control of graphene formation on nickel substrates^[17–21] and theoretical studies of carbon–metal system.^[22] The sample characterization is usually performed after synthesis, in a so-called “post-synthesis regime.” In our previous work^[23] we demonstrated such method for the production of graphene film with a controllable number of layers on nickel polycrystalline foils. But here we present the monitoring of synthesis process in a real-time regime.

This allows to get a deeper understanding of the mechanism of graphene growth on nickel substrate and to fabricate films containing an exact number of graphene layers (from three graphene layers to a thick graphite). The production of few-layer graphene with a desired thickness and accuracy gives an opportunity to use the samples in optical applications, such as saturable absorbing material.^[6,24–27]

For the first time, we show a possibility to control the decomposition of methane and the deposition of carbon onto nickel substrate using simple measurements of electrical resistance of the substrate foil. As it was described in literature^[11,13] the carbonaceous gas decomposes in presence of catalytic substrate at temperature of 400 °C or higher. Then the carbon atoms deposit onto metal substrate and begin to diffuse inside the bulk metal if the temperature increases beyond 650 °C. This process has not been yet observed experimentally. Here, we demonstrate the indirect estimation of the starting moment for the diffusion of carbon atoms into the bulk nickel. In our experiments we monitored the electrical resistance of nickel foil during the synthesis process after the methane introduction. As the carbon atoms start to diffuse inside the metal, its resistance changes rapidly. We were able to fix this moment in a real-time regime. The technical details of experiments and the discussion of the results are presented below.

Dr. M. G. Rybin, I. I. Kondrashov, A. S. Pozharov, Dr. E. D. Obraztsova
A.M. Prokhorov General Physics Institute
Vavilov str. 38, 119991 Moscow, Russia
E-mail: rybmaxim@gmail.com

Dr. M. G. Rybin, Dr. E. D. Obraztsova
National Research Nuclear University MEPhI (Moscow Engineering
Physics Institute)
31 Kashirskoye Shosse, 115409 Moscow, Russia

Dr. M. G. Rybin
Center for Functionalized Magnetic Materials (FunMagMa)
Immanuel Kant Baltic Federal University
14 A. Nevskogo ul., 236041 Kaliningrad, Russia

Dr. V. C. Nguyen, Prof. N. M. Phan
Institute of Materials Science
Vietnam Academy of Science and Technology
18 Hoang Quoc Viet, Hanoi, Vietnam

 The ORCID identification number(s) for the author(s) of this article can be found under <https://doi.org/10.1002/pssb.201700414>.

DOI: 10.1002/pssb.201700414

2. Experimental Details

All experiments were done using the original home-made equipment designed in the lab specially for CVD synthesis of graphene films. The chamber walls are cooled by water. The

main differences of the equipment from the commercial analogs (such as a CVD furnace quartz tube) are the following: i) the metal substrate is heated resistively by increasing the electrical current up to 100 A; ii) the temperature during the synthesis is measured through the window by an infrared pyrometer directly from the nickel substrate. A scheme of the setup is shown in **Figure 1a**. It provides the opportunity to control all of the synthesis parameters such as the heating and cooling rates, the temperature of substrate during the experiment, the gas pressure in the chamber and the gases concentrations. The most important feature of the setup is a possibility to measure the resistance of catalytic substrate during the experiments in a real-time mode. While the electrical current is increased for heating the metal foil, the power supply measures the voltage and, as a result, the computer software calculates the foil resistance by Ohm's law ($R = V/I$). The importance of these measurements is described in the next section of this paper.

As the experimental setup differs from the commercial analogs, the description of synthesis process is needed. Its scheme is presented in **Figure 1b**. The process of graphene synthesis goes in two steps: the preparation of nickel foil and the formation of graphene film. At the first stage the preparation of nickel substrate means its annealing. The foil with the size of 10×60 mm and the thickness of $25 \mu\text{m}$ is held between the electrodes in the chamber. The chamber is washed and filled to pressure up to 100–500 millibars with the mixture of argon and hydrogen in ratio 4:1. Then the substrate heating by passing a high electrical current is started. A linear current increase is monitored by the software. When the substrate temperature reaches the required value, the current increase is stopped. After this the temperature is held during the defined time. It was found that the rate of current increase, the temperature and the annealing time are very important, as they determine the size and quality of the grains produced in the polycrystalline nickel foil.^[13] In our experiments the heating rate is $60^\circ\text{C min}^{-1}$, the annealing temperature is 1050°C and the annealing time is 20 min. After annealing the substrate is cooled down to 750°C , the gases pumped out to get a required pressure and the next

stage of synthesis begins. It starts with the introduction of methane to obtain a desired concentration. After this the most important phase of synthesis starts. It is a gradual heating of the substrate by the electrical current increasing. During this heating the decomposition of methane and the deposition of amorphous carbon on the surface of the catalyst substrate take place under temperature higher than 500°C . The further diffusion of carbon into nickel starts at temperatures above 750°C .^[14] After stop of electrical current increase the requested temperature is kept for 20 min (similar to the procedure of annealing). Finally, the substrate is cooled down to the room temperature “instantaneously” (by turning off the electrical current). Graphene samples synthesized on nickel foils could be easily transferred onto arbitrary substrate using PMMA (Poly(methyl methacrylate)) as a supporting polymer substrate and nitric acid as an etchant. The polymer needs to cover graphene layer deposited on nickel. Then the metal substrate is etched in the solution (1 ml of HNO_3 in 5 ml of H_2O). Finally, the polymer with graphene is stack to the desired substrate and PMMA is dissolved in acetone (see **Figure 2**).

It should be noted that the most important stage of the synthesis is the heating of substrate after the introduction of methane as it is marked in **Figure 1b**. The temperature of substrate during the graphene fabrication is a general parameter. Thus, the key point of synthesis is the observation and control of the diffusion of carbon inside the bulk nickel. The discussion of the results are presented in the next section.

During the experimental investigation of the samples the Raman spectrometer Horiba LabRAM HR Evolution with 532 nm laser excitation wavelength and UV-Vis-NIR optical spectrometer Perkin Elmer Lambda 950 were used for characterization.

3. Results and Discussions

Our experiments were focused onto the study of mechanism of carbon deposition onto nickel substrate and further diffusion inside the bulk metal. As it is described above the experimental

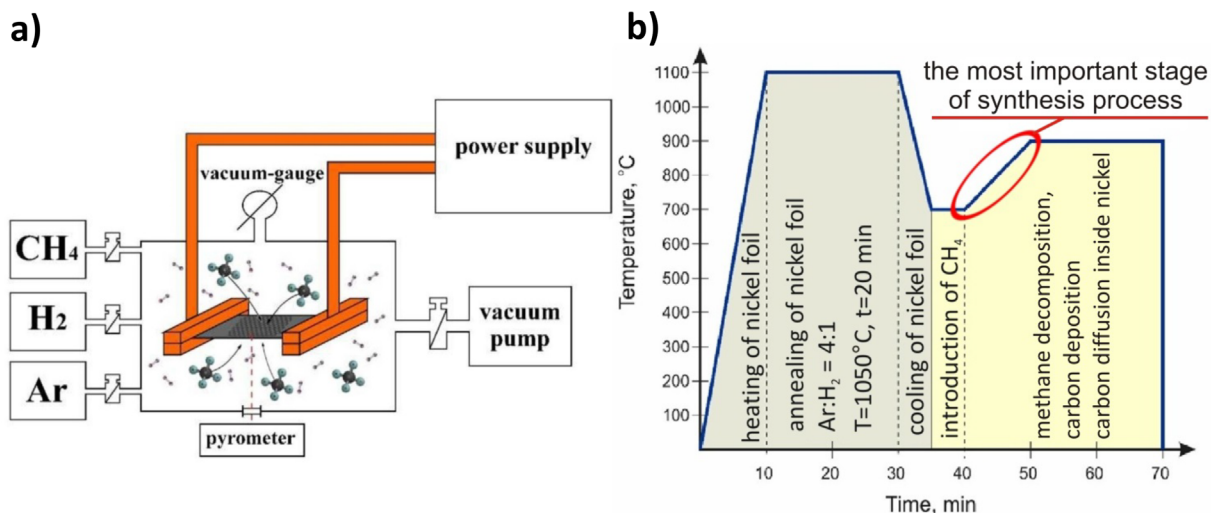


Figure 1. a) Scheme of CVD equipment for graphene synthesis; b) scheme of graphene synthesis process.

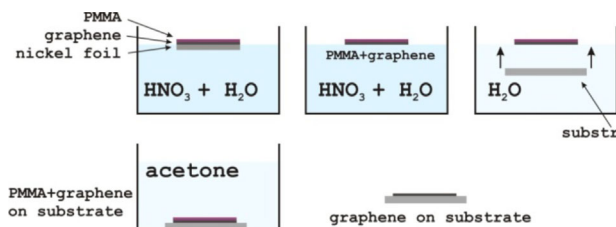


Figure 2. Scheme of transfer process of graphene films from nickel foils onto desired substrate.

equipment has a possibility to measure both the temperature of nickel foil and its electrical resistance during synthesis process in a real-time regime. Hence these measurements were used to control the process and, therefore, to produce graphene film with a desired thickness.

In Figure 1b the time period is marked as “the most important stage of synthesis process” because at this step we observe the diffusion of carbon inside nickel. After inlet of methane into reactor the heating of nickel foil by step-by-step increased electrical current is performed. It is well known that the electrical resistance of metal increases with the temperature. In the real-time regime the increase of resistance was observed, but in the critical point the resistance started to increase more rapidly, as evidenced from the change in the curve slope. In **Figure 3a** the resistance dependencies versus temperature of the nickel foils are presented by black and blue plots for methane concentration of 2 and 5%, respectively. Moreover, the critical temperature, corresponding to the breaking point in the temperature-dependent resistance, differs for different methane concentrations (for 2% of methane the critical temperature is 845 °C, and for 5% of methane it is 830 °C). We explain the change of dependence of electrical resistance on substrate temperature by the influence of diffused carbon atoms inside the nickel foil. More particularly, after the introduction of methane into chamber and the beginning of substrate heating,

the methane decomposes into hydrogen and carbon radicals, and the latter deposits onto nickel. This process does not influence on the resistance of nickel. But when the temperature reaches some point the carbon atoms deposited on the foil surface start to diffuse inside the nickel and to change the resistance versus temperature dependence of the metal. As it is known, in a pure metal the thermal vibrations of the lattice increases with the temperature, causing a more intensive electron scattering resulted in slowing down the electron flow. In case of penetration of carbon atoms between the atoms of metal crystalline lattice, the additional scattering of electrons occurs on carbon atoms. Hence the electrical resistance of nickel substrate with the diffused carbon atoms becomes larger than the resistance of the pure nickel foil. Moreover, the slope of $R(T)$ plot for the nickel foil is significantly higher after the carbon diffusion start (see the angles ψ and φ in **Figure 3a**). Using a simple function of temperature-dependent resistance of a pure metal,

$$R_1(T) = R_0 + aT, \quad (1)$$

where R_0 is a pure metal resistance at room temperature and a is a thermal coefficient, the formula for resistance of metal with embedded after diffusion carbon atoms can be represented as:

$$R_2(T) = \beta(R_0 + aT), \quad (2)$$

where β can be easily calculated from the plots in **Figure 3a**:

$$\beta = \psi_2/\psi_1 \quad \text{or} \quad \beta = \varphi_2/\varphi_1, \quad (3)$$

for 2% or 5% methane concentration, respectively. To calculate the exact value of thermal coefficient for nickel with embedded carbon atoms it is necessary to take into account the pressure in chamber during the synthesis process, but these calculations are not the challenge of present work. Also it should be noted that the diffusion of carbon is a non-linear process

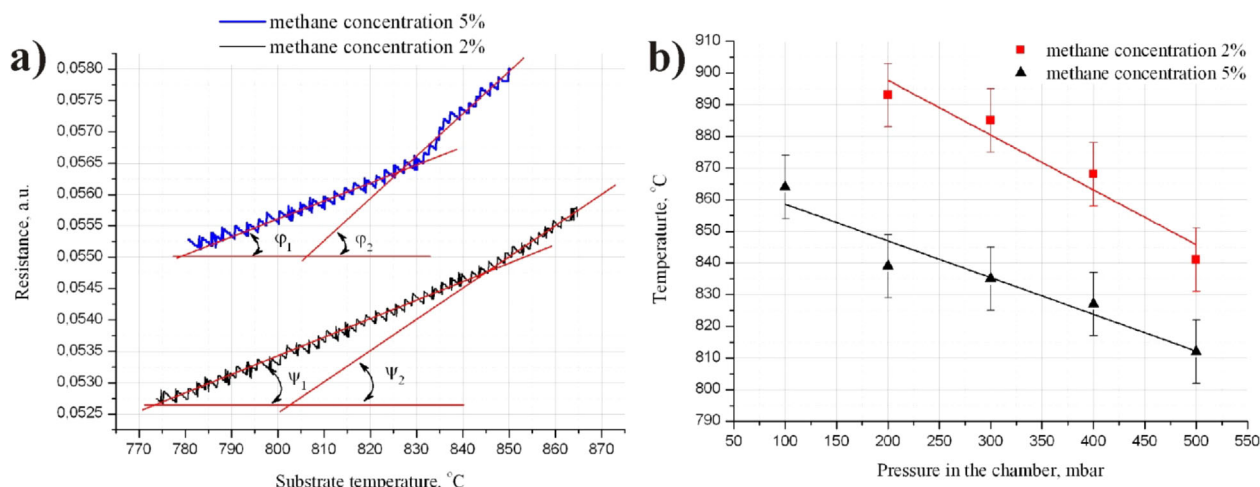


Figure 3. a) Dependences of electrical resistance of the nickel foil on its temperature after inlet of methane and starting the heating, where φ and ψ indicate the changes of the slopes of resistance versus temperature dependence (for two values of methane concentrations). b) Dependences of temperature of “diffusion start” on the gas pressure value in the chamber (for methane concentration of 2% and 5%).

and our linear approximation can be applied only for a small amount of diffused carbon and for the temperatures of 50–70 degrees after the diffusion start. The coefficient β becomes dependent on the substrate temperature. Such investigation is more complicated and is not in the field of our investigation.

In addition it was found that the temperature of the substrate, corresponding to the start of diffusion process, depends on the methane concentration and the pressure in the chamber (the corresponding dependence are presented in Figure 3b). As it can be seen from the figure, this temperature increases with decreasing of methane concentration and with decreasing of pressure in the chamber. Thereby the higher the amount of methane in the chamber, the lower the temperature of diffusion start.

Basing on results of these experiments and on the published data concerning a nickel-carbon system^[13] we propose that the beginning of diffusion of carbon atoms inside the bulk nickel at different temperatures occurs due to combination of three types of contributions: i) the catalytic activity of nickel increases rapidly at certain temperature; ii) the thermal extension of nickel crystalline lattice allows to accept inside a huge amount of carbon atoms delivered via diffusion; iii) the diffusion rate of carbon into nickel increases rapidly at certain temperature. Thus, the information about the beginning of carbon diffusion provides a possibility to control comparatively the amount of carbon atoms penetrated inside the bulk nickel by monitoring the time period after the diffusion start or by controlling the temperature of the nickel foils after the diffusion start. The

increase of the substrate temperature after the diffusion start results in the increase of amount of carbon atoms penetrated inside nickel. Thereby the higher is the temperature of nickel substrate, the larger is the number of carbon atoms diffused in nickel, resulting in the thicker graphene film formed after the substrate cooling down to the room temperature (see Figure 4a). For instance, the trilayer graphene film can be obtained in case when the maximum temperature of nickel foil is 30 degrees higher than the temperature of diffusion start (for methane concentration of 2% and gas pressure in the chamber of 500 mbar).

The fabricated graphene samples were transferred onto the quartz substrate (for optical absorption measurements) and onto the 300 nm-oxide layer covered silicon substrate (for Raman measurements). The photos of transferred thin graphene films and the corresponding optical transmittance and Raman spectra are shown in Figure 4b–d. It can be seen from the photographs (Figure 4b) that the graphene films are not perfectly uniform. This is a result of temperature inhomogeneity over the nickel foil during synthesis. The temperature of nickel substrate influences to the amount of diffused carbon atoms and to the thickness of graphene film. Thereby a low change of temperature over the foil results in some irregularity of graphene film. The Raman and optical absorption spectra were measured from the thickest points of graphene films. The Raman spectrum of 20-layers graphene (Figure 4c) confirms the high quality of synthesized films by a negligible D-peak at 1350 cm^{-1} , a high and narrow G-peak at 1582 cm^{-1} and a presence of 2D-band around 2700 cm^{-1} with the full width at half maximum (FWHM) of

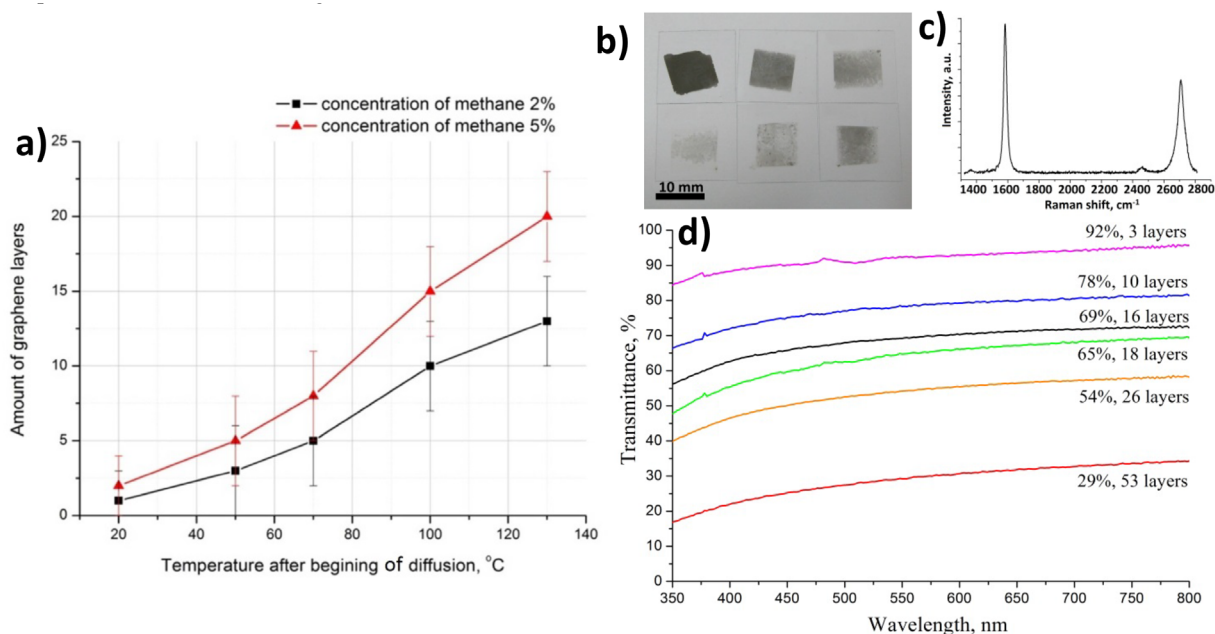


Figure 4. a) Temperature-dependences of thickness of graphene films on nickel foil after the carbon diffusion start for pressure of 500 mbar. b) Photo of graphene films on quartz substrates with the thicknesses ranged from 3 to 53 layers (the lateral sizes of graphene films are $10 \times 10\text{ mm}^2$). c) Raman spectrum of film containing 20 graphene layers (under the laser excitation of 532 nm). d) Optical transmittance spectra of films containing different numbers of graphene layers, corresponding to photographs in figure b. (The numbers of layers have been calculated taking into account the absorbance of single graphene layer of 2.3% of incident light intensity at 550 nm).

50 cm⁻¹. The optical absorption spectra of synthesized graphene films are presented in Figure 4d. The number of graphene layers n in films have been calculated taking into account the absorption of single graphene layer of 2.3% of incident light intensity at 550 nm:

$$n = \log_{0.977} t, \quad (4)$$

where 0.977 is the transmittance of graphene monolayer and t is total transmittance of the film. Therefore it is easy to obtain a graphene film with a desired thickness from 3 to 50 layers and more.

4. Conclusions

The fabrication of high-quality monolayer graphene on copper foils is reported in literature as a solved problem. But revealing the mechanism of graphene formation on nickel foil and the realization of real-time controlled synthesis of multi-layered graphene film on nickel are still interesting and important tasks. This process provides the formation of graphene film with a desired thickness for optical applications. Here we have demonstrated an original approach for the in situ control of graphene synthesis by monitoring the carbon–nickel system through temperature-dependent electrical resistance measurements. It has been shown that the solubility of carbon in bulk nickel can be controlled in a real-time regime and, as a result, the graphene films can be grown with desired thicknesses. The solubility of carbon in nickel results in the diffusion of carbon atoms inside the nickel crystalline lattice and influences the electrical resistance of the nickel foil. By monitoring the temperature-dependent electrical resistance of nickel foil, both the amount of carbon atoms diffused inside the nickel foil and the thickness of graphene film after cooling can be controlled. The synthesis of graphene films with thickness from 3 to 53 layers has been demonstrated.

Acknowledgements

The reported study was funded by RFBR, according to the research projects No. 16-32-60203 mol_a_dk and No. 16-52-540003 Viet_a. This work was supported by the Competitiveness Programm of NRNU MEPhI.

Conflict of Interest

The authors declare no conflict of interest.

Keywords

chemical vapor deposition, foils, graphene, Joule heating, nickel, optical absorption spectroscopy

Received: August 2, 2017
Revised: October 19, 2017
Published online: November 17, 2017

- [1] S. J. Kim, K. Choi, B. Lee, Y. Kimand, B. H. Honget, *Rev. Mater. Res.* **2015**, *45*, 63.
- [2] E. O. Polat, O. Balci, N. Kakenov, H. B. Uzlu, C. Kocabas, R. Dahiyaet, *Sci. Rep.* **2015**, *5*, 16744.
- [3] K. S. Novoselov, V. I. Fal'ko, L. Colombo, P. R. Gellert, M. G. Schwab, K. Kim, *Nature* **2012**, *490*, 192.
- [4] A. Ferrari, F. Bonaccorso, V. Fal'ko, K. S. Novoselov, S. Roche, P. Bøggild, S. Borini, F. H. L. Koppens, V. Palermo, N. Pugno, J. A. Garrido, R. Sordan, A. Bianco, L. Ballerini, M. Prato, E. Lidorikis, J. Kivioja, C. Marinelli, T. Ryhänen, A. Morpurgo, J. N. Coleman, V. Nicolosi, L. Colombo, A. Fert, M. Garcia-Hernandez, A. Bachtold, G. F. Schneider, F. Guinea, C. Dekker, M. Barbone, Z. Sun, C. Galiotis, A. N. Grigorenko, G. Konstantatos, A. Kis, M. Katsnelson, L. Vandersypen, A. Loiseau, V. Morandi, D. Neumaier, E. Treossi, V. Pellegrini, M. Polini, A. Tredicucci, G. M. Williams, B. H. Hong, J.-H. Ahn, J. M. Kim, H. Zirath, B. J. van Wees, H. van der Zant, L. Occhipinti, A. Di Matteo, I. A. Kinloch, T. Seyller, E. Quesnel, X. Feng, K. Teo, N. Rupesinghe, P. Hakonen, S. R. T. Neil, Q. Tannock, T. Löfwanderaq, J. Kinaret, *Nanoscale* **2015**, *7*, 4598.
- [5] Qi. Bao, K. P. Loh, *ACS Nano* **2012**, *6*, 3677.
- [6] V. R. Sorochenko, E. D. Obratsova, P. S. Rusakov, M. G. Rybin, *Quantum Electron.* **2012**, *42*, 907.
- [7] A. Y. Bykov, T. V. Murzina, M. G. Rybin, E. D. Obratsova, *Phys. Rev. B* **2012**, *85*, 121413(R).
- [8] P. A. Obratsov, M. G. Rybin, A. V. Tyurnina, S. V. Garnov, E. D. Obratsova, A. N. Obratsov, Y. P. Svirko, *Nano Lett.* **2011**, *11*, 1540.
- [9] E. D. Obratsova, M. G. Rybin, P. A. Obratsov, in: *Carbon Photonics*, V. Konov (Ed.), Nauka, Moscow **2017**.
- [10] M. G. Rybin, A. S. Pozharov, C. Chevalier, M. Garrigues, C. Seassal, R. Peretti, C. Jamois, P. Viktorovitch, E. D. Obratsova, *Phys. Status Solidi B* **2012**, *249*, 2530.
- [11] R. Muñoz, C. Gómez-Aleixandre, *Chem. Vap. Deposit.* **2013**, *19*, 297.
- [12] C. Mattevi, H. Kima, M. Chhowalla, *J. Mater. Chem.* **2011**, *21*, 3324.
- [13] A. Dahala, M. Batzill, *Nanoscale* **2014**, *6*, 2548.
- [14] J. J. Lander, H. E. Kern, A. L. Beach, *J. Appl. Phys.* **1952**, *23*, 1305.
- [15] C. Bernardo, L. S. Lobo, *Carbon* **1976**, *14*, 287.
- [16] M. Singleton, P. Nash, *J. Phase Equilib.* **1989**, *10*, 121.
- [17] A. Umair, H. Raza, *Nanoscale Res. Lett.* **2012**, *7*, 437.
- [18] A. Reina, X. Jia, J. Ho, D. Nezich, H. Son, V. Bulovic, M. S. Dresselhaus, J. Kong, *Nano Lett.* **2009**, *9*, 30.
- [19] L. Huang, Q. H. Chang, G. L. Guo, Y. Liu, Y. Q. Xie, T. Wang, B. Ling, H. F. Yang, *Carbon* **2012**, *50*, 551.
- [20] R. S. Weatherup, B. Dlubak, S. Hofmann, *ACS Nano* **2012**, *6*, 9996.
- [21] Q. Yu, J. Lian, S. Siriponglert, H. Li, Y. P. Chen, S.-S. Pei, *Appl. Phys. Lett.* **2008**, *93*, 113103.
- [22] P. V. Shvets, A. N. Obratsov, *J. Nanophoton.* **2016**, *10*, 012506.
- [23] M. Rybin, A. Pozharov, E. Obratsova, *Phys. Status Solidi C* **2010**, *7*, 2785.
- [24] Q. Bao, H. Zhang, Y. Wang, Z. Ni, Y. Yan, Z. X. Shen, K. P. Loh, D. Y. Tang, *Adv. Funct. Mater.* **2009**, *19*, 3077.
- [25] Z. Sun, T. Hasan, F. Torrisi, D. Popa, G. Privitera, F. Wang, F. Bonaccorso, D. M. Basko, A. C. Ferrari, *ACS Nano* **2010**, *4*, 803.
- [26] K. Y. Lau, F. D. Muhammad, A. A. Latif, M. H. Abu Bakara, Z. Yusoff, M. A. Mahdi, *Opt. Laser Technol.* **2017**, *94*, 221.
- [27] G. Sobon, J. Sotor, I. Pasternak, A. Krajewska, W. Strupinski, K. M. Abramski, *Opt. Mater. Express* **2015**, *5*, 2884.